

Antitumor Agents

How to cite: *Angew. Chem. Int. Ed.* **2020**, *59*, 14677–14685

International Edition: doi.org/10.1002/anie.202006814

German Edition: doi.org/10.1002/ange.202006814

Glycoconjugated Metallohelicenes have Improved Nuclear Delivery and Suppress Tumour Growth In Vivo

Hualong Song, Simon J. Allison, Viktor Brabec,* Hannah E. Bridgewater, Jana Kasparikova, Hana Kostrhunova, Vojtech Novohradsky, Roger M. Phillips,* Jitka Pracharova, Nicola J. Rogers,* Samantha L. Shepherd, and Peter Scott*

Abstract: Monosaccharides are added to the hydrophilic face of a self-assembled asymmetric Fe^{II} metallohelix, using CuAAC chemistry. The sixteen resulting architectures are water-stable and optically pure, and exhibit improved anti-proliferative selectivity against colon cancer cells (HCT116 p53^{+/+}) with respect to the non-cancerous ARPE-19 cell line. While the most selective compound is a glucose-appended enantiomer, its cellular entry is not mainly glucose transporter-mediated. Glucose conjugation nevertheless increases nuclear delivery ca 2.5-fold, and a non-destructive interaction with DNA is indicated. Addition of the glucose units affects the binding orientation of the metallohelix to naked DNA, but does not substantially alter the overall affinity. In a mouse model, the glucose conjugated compound was far better tolerated, and tumour growth delays for the parent compound (2.6 d) were improved to 4.3 d; performance as good as cisplatin but with the advantage of no weight loss in the subjects.

Introduction

We have developed several structurally distinct ranges of metallohelicenes comprising three organic ligands that encapsulate two metal ions,^[1] such as that shown in Scheme 1a. Unlike conventional helicates,^[2] these water-stable Fe^{II} compounds self-assemble as optically pure architectures, principally a result of inter-ligand steric and secondary interactions including hydrophobic π -stacks.^[3] There is mounting evidence that as a result of their charge, shape, size and amphipathic structures, these compounds emulate some of the functional properties of short cationic α -helical peptides. Oriented binding to various nucleic acid structures is observed.^[1a,4] One class^[1b] inhibits ice recrystallization apparently as a result of the facially amphipathic architecture that is also present in natural antifreeze peptides.^[5] A similar structure binds to the central hydrophobic α -helical region of an amyloid β protein and attenuates toxicity.^[6] Perhaps most convincingly, we showed recently that a class of antimicrobial metallohelix in our library^[1c] rapidly penetrates the formidable cell envelope of a clinically-relevant Gram negative microbe and causes a peptide-like genomic and transcriptomic response.

Cell-penetrating peptides (CPPs) are usually relatively short (5–50 residues)^[7] and contain an excess of cationic amino acids (lysine and arginine).^[8] It is proposed that they pass through the plasma membrane via an ion exchange mechanism^[9] using negatively charged species such as anionic lipids and glycosaminoglycans. Since these components are in excess in cancer cell and microbial outer-leaflets,^[10] a generalized source of selectivity over other cells is provided. Nevertheless, such polycationic molecules may also have non-specific affinity for a number of biomolecular structures^[7,11] and the modification of CPPs with biocompatible fragments has been used in an attempt to modulate the attendant toxicity.^[11b,12] In particular, glycoconjugation has been used extensively for the modification of potential therapeutics of a number of kinds.^[13] In nature, glycosylation is one of the most common post-translational modifications^[14] and glycopeptides are involved in cell signalling,^[15] providing cell surface markers for recognition, and immune response.^[16] From a drug-design perspective, monosaccharide-conjugated analogues have been reported in the literature since the early 1990s,^[17] improving the water solubility and serum stability of their cargo,^[17b] as well as altering drug metabolism and pharmacokinetics (DMPK)^[18] including some literature precedent for exploiting the Warburg effect in cancer therapy.^[19]

[*] Dr. H. Song, Dr. H. E. Bridgewater, Dr. N. J. Rogers, Prof. P. Scott
Department of Chemistry, University of Warwick
Coventry, CV4 7AL (UK)
E-mail: Nicola.Rogers@warwick.ac.uk
Peter.Scott@warwick.ac.uk

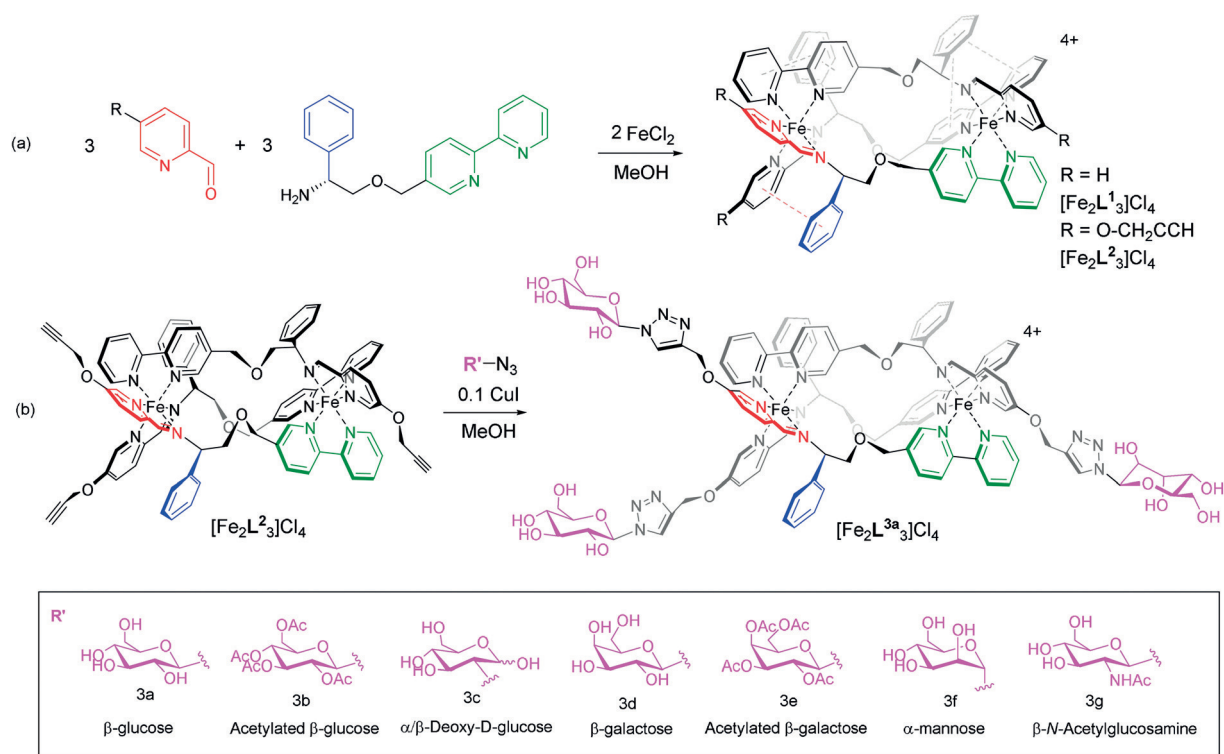
Dr. S. J. Allison, Prof. R. M. Phillips, Dr. S. L. Shepherd
School of Applied Sciences, University of Huddersfield
Huddersfield, HD1 3DH (UK)
E-mail: R.M.Phillips@warwick.ac.uk

Prof. V. Brabec, Prof. J. Kasparikova, Dr. H. Kostrhunova,
Dr. V. Novohradsky, Dr. J. Pracharova
The Czech Academy of Sciences, Institute of Biophysics
Kralovopolska 135, 61265 Brno (Czech Republic)
E-mail: Brabec@ibp.cz

Dr. J. Pracharova
Department of Biophysics, Centre of the Region Hana for Biotechnological and Agricultural Research, Faculty of Science, Palacký University
Šlechtitelů 27, 78371 Olomouc (Czech Republic)

Supporting information and the ORCID identification number(s) for the author(s) of this article can be found under <https://doi.org/10.1002/anie.202006814>.

© 2020 The Authors. Published by Wiley-VCH Verlag GmbH & Co. KGaA. This is an open access article under the terms of the Creative Commons Attribution License, which permits use, distribution and reproduction in any medium, provided the original work is properly cited.



Scheme 1. Synthesis of new sugar-functionalised metallohelices, using CuAAC post-assembly modification of self-assembled triplex metallohelices.

Several groups have also shown that glycosylation of a peptide increases membrane penetration, including through the blood–brain barrier.^[20] In recent work, Montenegro and co-workers developed a strategy for the glycosylation of short peptides, and have systematically characterized the uptake efficiency and distribution in various cell lines.^[21]

Our recent success in CuAAC derivatization of metallohelices using relatively simple functionality,^[1d] and an in cellulose click staining protocol,^[1e] gave us confidence to attempt the rather more ambitious glycoconjugations. We report here that this chemistry, giving rise to some of the most complex functionalized metallosupramolecular structures known, proceeds smoothly and efficiently, leading to improved cancer-cell targeting in vitro, and improved efficacy in vivo.

Results and Discussion

Selection of metallohelix system

The position of hydrophobic regions within a peptide is conventionally assessed by a simple residue-based approach, but this is not applicable here. Instead, analysis^[5] (Figure S1 in the Supporting Information) of the position of counter-anions in the solid state molecular structure reveals a favorable charge distribution for one of our so-called triplex^[1b] architectures (Scheme 1) in that the two π -stacked arene rings, colored pink in Figure 1, shield the cationic charge, leading to the creation of a relatively hydrophobic upper ridge. A

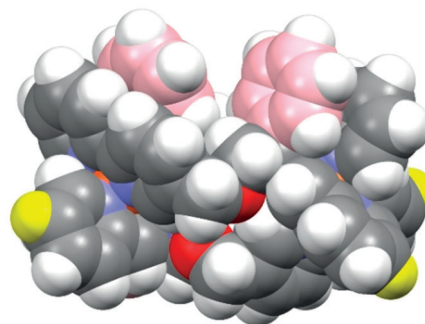


Figure 1. Schematic representation of $[M_2L_3]^{4+}$ architecture. Space-fill model based on a previously reported structure.^[1b] Note the two π -stacked arenes colored in pink on the upper hydrophobic edge. The H atoms colored in yellow correspond to the positions of the R groups attached on the lower hydrophilic face.

third π -stack is hidden at the rear of this view. The yellow colored atoms correspond to the positions of groups R in Scheme 1; they will surround a relatively hydrophilic face and hence by adding sugar units at these latter positions we retain the amphipathic architecture. This, we considered, was the approach most likely to allow retention of the kinds of biological activity we have seen from the core structure, while allowing us to test the idea that glycosylation may lead to improvements in delivery, selectivity and tolerance.

Synthesis and characterization

The starting materials for new synthesis were assembled: the previously-reported^[1d] enantiomerically pure triplex metallohelix $[\text{Fe}_2\text{L}^2_3]\text{Cl}_4$ with alkynyl groups at the positions colored yellow in Figure 1 was prepared on a multi-g scale via a one-pot highly diastereoselective self-assembly reaction; the range of monosaccharide azides of Scheme 1b, including acylated analogues, were synthesized by literature procedures.^[22]

The subsequent CuAAC glycosylation was not initially straightforward. The conventional copper sulfate/sodium ascorbate catalyst led to difficulties in isolation in this rather polar system, while the heterogeneous catalyst copper-in-charcoal^[23] failed to complete the reaction. We considered the copper free click reaction^[24] but the requirement for cyclooctyne groups would significantly increase the synthetic challenge and restrict versatility. Eventually we found to our surprise that while copper(I) iodide catalyst required elevated temperatures, this was not deleterious, the reactions were complete, and the work-up was trivial. This gave us access to the glycoconjugated triplex metallohelices $[\text{Fe}_2\text{L}^{3a-8}_3]\text{Cl}_4$ as optically pure isolated compounds.

The success of this post-assembly CuAAC is apparent from the ¹H-NMR spectra (Figure 2A and B; for all spectra see Figure S2–S9). For example, the singlets H^j at ca 3 ppm corresponding to the three inequivalent alkyne units in the starting material are cleanly replaced by three new singlets at 8.06, 8.17, and 8.28 ppm (H^m) for the triazole rings in the product. It is also noteworthy that the two bipyridine protons involved in inter-strand hydrogen bonds, and thus giving rather low field resonances (ca 9.2 ppm), are present in both starting material and product, confirming that the asymmetric triplex architecture is unperturbed by the presence of the sugars. High resolution electrospray mass spectra were readily obtained; Figure 2C shows the expected tetracationic molecular ion pattern for $S_c, \Lambda_{\text{Fe}}\text{-HHT-}[\text{Fe}_2\text{L}^{3a}_3]\text{Cl}_4$. The circular dichroism (CD) spectra of the diastereoisomers (Figure 2D) $\Lambda\text{-}[\text{Fe}_2\text{L}^{3a}_3]\text{Cl}_4$ and $\Delta\text{-}[\text{Fe}_2\text{L}^{3a}_3]\text{Cl}_4$ in H_2O display peaks of opposite molar differential extinction coefficients, and mimic the features of the enantiomeric pairs of $[\text{Fe}_2\text{L}^1_3]\text{Cl}_4$ and $[\text{Fe}_2\text{L}^2_3]\text{Cl}_4$.^[1d]

The glycoconjugated compounds were found to be extraordinarily stable under aqueous conditions; no decomposition was observed on monitoring the absorption at the MLCT band in aqueous solution over many months, and even when dissolved in KCl/HCl buffer at pH 1.5 (at 8 mM) no decomposition was observed over one month (Figure S18).

Antiproliferative activity and cell studies

The whole panel of Fe^{II} compounds of Scheme 1 were evaluated alongside cisplatin for potency against the human colorectal cancer cells with wild-type p53 (HCT116 p53^{+/+}) and non-cancerous human epithelial retinal pigment cells (ARPE-19) (Figure 3).

We observe that the sugar-appended triplex systems all inhibit HCT116 p53^{+/+} cell proliferation in the 2–30 μM

concentration range (96 h IC_{50}), and for all examples the Λ -diastereoisomers are more potent than Δ . The selectivity indices (SI, defined as $\text{IC}_{50}[\text{ARPE19}]/\text{IC}_{50}[\text{HCT116 p53}^{+/+}]$) vary from 1.4 to 17, with greater selectivity observed most often with the Δ -diastereoisomers. With SI of 17, $\Delta\text{-}[\text{Fe}_2\text{L}^{3a}_3]\text{Cl}_4$ is the most selective compound in the panel for this pair of cells. Since this indicates a potential therapeutic window, we chose to focus on this compound for more detailed study.

We compared the antiproliferative activity of $\Delta\text{-}[\text{Fe}_2\text{L}^{3a}_3]\text{Cl}_4$ in both glucose-rich and glucose-free media and observed no difference in IC_{50} (Table S2). We further incubated the drug with GLUT-1 overexpressing MCF-7 breast cancer cells and compared the IC_{50} with wild type MCF-7 cells and found that rather than being more sensitive to the glucose derivative, the GLUT-1 overexpressing cells are actually *ca* three-fold more resistant (Table S3). Firstly, this suggests that the cellular entry of these compounds is not (or not mainly) GLUT-mediated; given the specificity of binding of this receptor this is perhaps unsurprising, but the addition of glucose units to large molecules has been nevertheless described as a cancer cell-targeting strategy.^[17b,25] Secondly, we note that the resistance we observed may be beneficial in that normal cells that have high GLUT-1 expression (e.g. red blood cells) will be less adversely affected.

The conjugation of sugars with therapeutic peptides and other drug candidates can alter pharmacokinetic properties, and has been demonstrated to improve physiological properties and bioavailability,^[26] such as enhancing biodistribution in tissues,^[27] improving membrane penetration^[28] and targeted delivery.^[29] We therefore firstly compared the effects of $\Delta\text{-}[\text{Fe}_2\text{L}^1_3]\text{Cl}_4$ and the glycosylated analogue $\Delta\text{-}[\text{Fe}_2\text{L}^{3a}_3]\text{Cl}_4$ on the cell cycle in HCT116 p53^{+/+} cells, which were treated at different concentrations for 24 h and then evaluated via flow cytometry.

As shown in Figure 4, $\Delta\text{-}[\text{Fe}_2\text{L}^1_3]\text{Cl}_4$ induces a decrease in the proportion of cells in the G2/M phase (green), whereas in cells treated with $\Delta\text{-}[\text{Fe}_2\text{L}^{3a}_3]\text{Cl}_4$ this remains unchanged even up to 20 μM . Correspondingly, $\Delta\text{-}[\text{Fe}_2\text{L}^1_3]\text{Cl}_4$ causes a slight dose-dependent increase in the proportion of cells in the G1 and S phases of the cell cycle. In distinct contrast, $\Delta\text{-}[\text{Fe}_2\text{L}^{3a}_3]\text{Cl}_4$ induces a dose-dependent loss of the number of cells in G1 phase in favor of S phase. These findings indicate a change in mechanisms of action upon attaching the glucose unit to the triplex metallohelix. The counts associated with the sub-G1 phase were also analyzed; the increasing amount of cell material indicates a growing number of cells undergoing cell death, with $\Delta\text{-}[\text{Fe}_2\text{L}^1_3]\text{Cl}_4$ inducing greater cell death than $\Delta\text{-}[\text{Fe}_2\text{L}^{3a}_3]\text{Cl}_4$.

We also compared the cellular accumulation of $\Delta\text{-}[\text{Fe}_2\text{L}^{3a}_3]\text{Cl}_4$ with that of $\Delta\text{-}[\text{Fe}_2\text{L}^1_3]\text{Cl}_4$; HCT116 p53^{+/+} cells were incubated with metallohelix (5 μM) for 16 h, and Fe content was determined using ICP-MS, with Fe counts for untreated control cells subtracted as a baseline from all samples. In addition, we determined the nuclear uptake of $\Delta\text{-}[\text{Fe}_2\text{L}^1_3]\text{Cl}_4$ and $\Delta\text{-}[\text{Fe}_2\text{L}^{3a}_3]\text{Cl}_4$ under the same conditions using a Nuclei EZ Prep (Sigma–Aldrich) nuclei isolation kit.

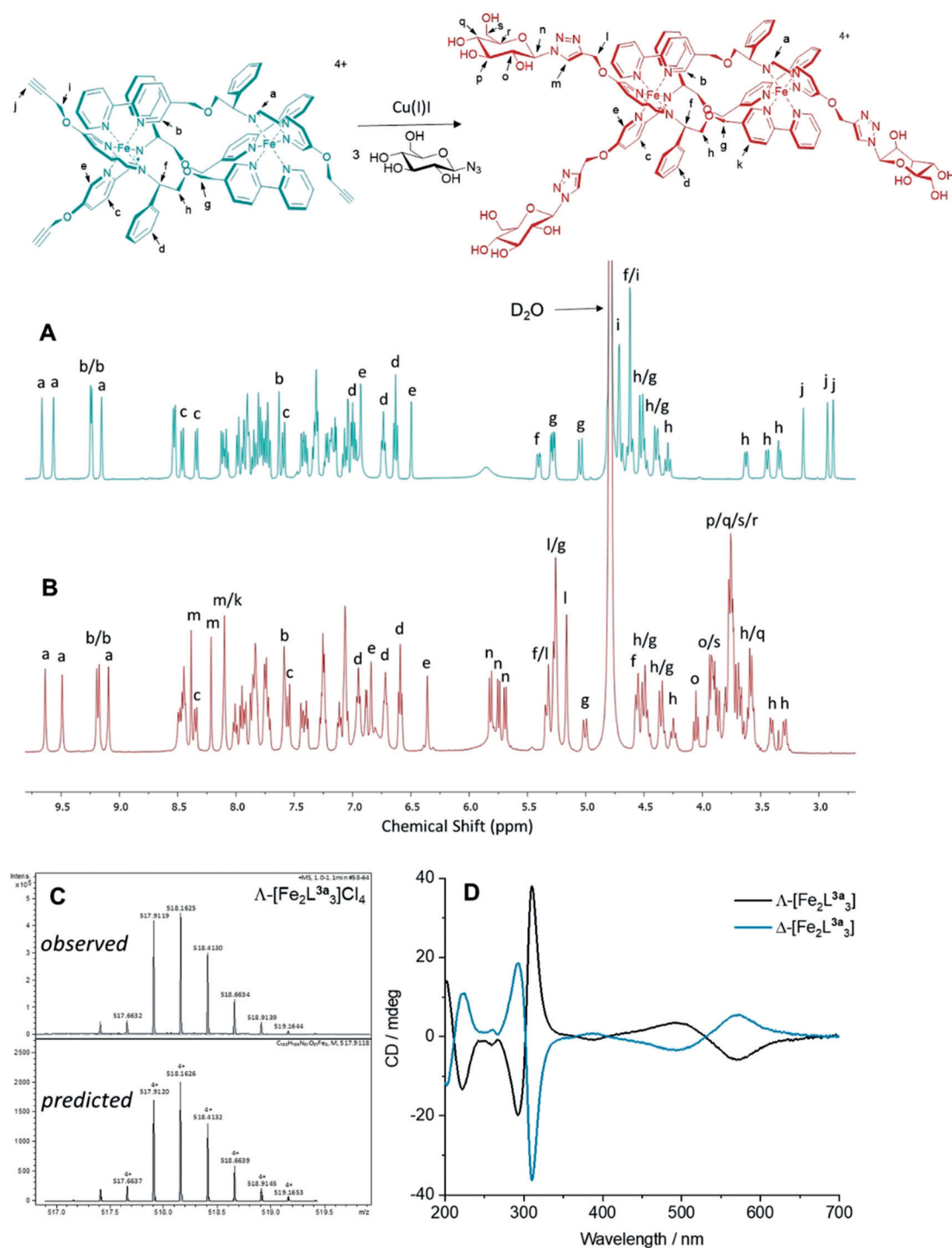


Figure 2. Characterization of glucose-functionalized triplex metallohelices. A) ¹H NMR (500 MHz, D₂O, 298 K) of the precursor complex Δ -[Fe₂L₂³]₃Cl₄ (cyan), and B) of the product Δ -[Fe₂L_{3^a]₃Cl₄ (red) following CuAAC. C) High resolution ESI mass spectrum of Δ -[Fe₂L_{3^a]₃Cl₄ showing the observed $z = +4$ charge (top), compared to the theoretical isotope pattern (bottom). D) Circular dichroism spectra of Δ -[Fe₂L_{3^a]₃Cl₄ (black) and Δ -[Fe₂L_{3^a]₃Cl₄ (blue) (40 μ M in H₂O).}}}}

Accumulation of 21.9 ± 2.1 pmol Fe/10⁶ cells was observed following incubation with Δ -[Fe₂L₁³]₃Cl₄ and 15.9 ± 2.7 pmol Fe/10⁶ cells with Δ -[Fe₂L_{3^a]₃Cl₄ (Figure 5 A). Despite the lower cellular uptake of Δ -[Fe₂L_{3^a]₃Cl₄ compared to Δ -[Fe₂L₁³]₃Cl₄ (ca 73 %), 2.5 times more Fe was localized in the nucleus; only 4% of the total ion uptake was associated with}}

the nuclei for the parent triplex Δ -[Fe₂L₁³]₃Cl₄, whereas 12% was observed for the sugar-conjugate Δ -[Fe₂L_{3^a]₃Cl₄.}

To confirm this observation, the intracellular compartmentalization of Δ -[Fe₂L₁³]₃Cl₄ and Δ -[Fe₂L_{3^a]₃Cl₄ in HCT116 p53^{+/+} was also investigated using a FractionPREP™ Cell Fractionation kit (BioVision) to isolate four sub-cellular}

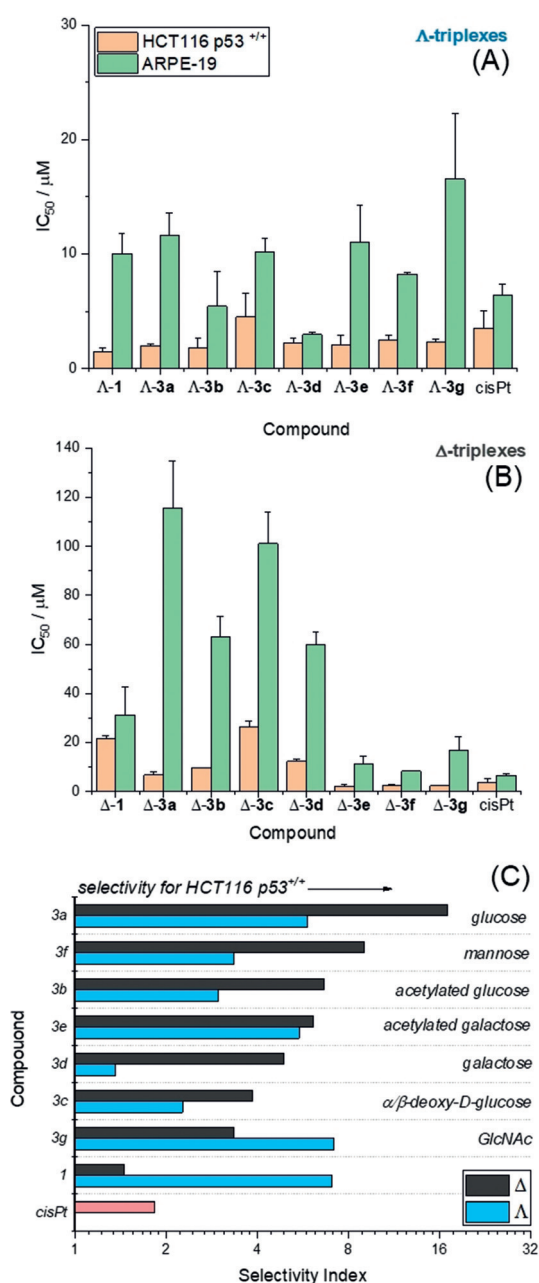


Figure 3. Antiproliferative activity of triplex metallohelices in cancer and non-cancer cells. The half maximum inhibitory concentration (IC_{50}) values are measured in triplicate by MTT assay, dosing for 96 h against HCT116 p53^{+/+} and ARPE-19 cells. A) Δ -triplex metallohelices; B) Δ -triplex metallohelices. The selectivity index C) defined as [mean IC_{50} (ARPE-19)]/[mean IC_{50} (HCT116 p53^{+/+})] for the clinical drug cisplatin (cisPt), the “parent” triplex $[Fe_2L^1_3]Cl_4$ and CuAAC-derived sugar systems $[Fe_2L^{3a-g}]Cl_4$.

fractions: (i) cytoskeletal fraction (total cellular insoluble proteins) plus genomic DNA), (ii) nuclear fraction (nuclear soluble proteins, including nuclear membrane proteins), (iii) membrane fraction (organelles and organelle membrane proteins, but excluding nuclear membrane proteins), and (iv) cytosolic fraction (total cytoplasmic soluble proteins). The cells were grown and treated as above and Fe content was again determined by ICP-MS. As shown in Figure 5B, the

localization of Δ - $[Fe_2L^{3a}]Cl_4$ in the nuclear fraction (13.6%) was more pronounced in comparison with Δ - $[Fe_2L^1_3]Cl_4$ (4.4%), and was consistent with the data observed in Figure 5A. Both Δ - $[Fe_2L^1_3]Cl_4$ and Δ - $[Fe_2L^{3a}]Cl_4$ distribute most predominantly in the membrane fraction at 16 h (62.0% and 55.7% respectively), whereas the localization of Δ - $[Fe_2L^1_3]Cl_4$ (25.3%) in the cytoskeleton fraction is more significant than for Δ - $[Fe_2L^{3a}]Cl_4$ (19.6%). There are several reports of glycosylation-dependent nuclear import of proteins and plasmids,^[30] which could be related to the cytosol-nuclear lectins shuttling between the cytosol and the nucleus.^[30c]

Single-cell gel electrophoresis studies (Comet Assay) in HCT116 p53^{+/+} cells treated with Δ - $[Fe_2L^{3a}]Cl_4$ revealed an absence of single- or double- strand DNA breaks due to the lack of a “comet” tail (Figure 5C). In addition, Δ - $[Fe_2L^{3a}]Cl_4$ does not retard the formation of the “comets” in cells treated with DNA damaging peroxide, indicating that it does not form DNA cross-links. The parent compound Δ - $[Fe_2L^1_3]Cl_4$ behaves similarly.^[1b] Thus if these metallohelices interact with DNA in the nucleus, they do not cause irreversible changes leading to cell death, as does cisplatin.^[31]

Notwithstanding these findings, we compared the antiproliferative activity of these complexes in the pair of Chinese Hamster Ovary Cell lines CHO-K1 and MMC-2 (Table 1); a system previously used to identify the DNA damage involvement of cytotoxic agents. MMC-2 is a CHO-K1 mutant carrying the ERCC3/XPB mutation, which renders this cell line deficient in DNA nucleotide excision repair (NER).^[32]

The factor F (Table 1), which compares IC_{50} for Chinese Hamster Ovary cells (wild type) and the NER deficient system, is rather lower for Δ - $[Fe_2L^1_3]Cl_4$ and Δ - $[Fe_2L^{3a}]Cl_4$ than it is for the DNA damaging agent cisplatin, but there is a three or six-fold difference between the response of the two cell lines; this prompted us to study DNA interactions in vitro (below). We further compared the antiproliferative activity of Δ - $[Fe_2L^1_3]Cl_4$ and Δ - $[Fe_2L^{3a}]Cl_4$ against A2780 ovarian cancer cells, and the cisplatin-resistant strain A2780cisR (Table 2). No cross-resistance with cisplatin was detected. We also compared the response of p53-deficient and wild type HCT116 cells. Whilst p53-deficient cells were less responsive to cisplatin, there was no significant difference between the response of HCT116 p53^{+/+} and p53^{-/-} cells ($p > 0.05$) in the case of Δ - $[Fe_2L^{3a}]Cl_4$, with Δ - $[Fe_2L^1_3]Cl_4$ demonstrating significantly ($p < 0.01$) enhanced activity against p53 deficient cells. Together these data are consistent with both Δ - $[Fe_2L^1_3]Cl_4$ and Δ - $[Fe_2L^{3a}]Cl_4$ inducing their antiproliferative

Table 1: Antiproliferative data (IC_{50}) determined by MTT test for CHO-K1 (wild-type) and MMC-2 (NER-deficient).^[a]

Compound	CHO-K1	MMC-2	F ^[b]
Δ - $[Fe_2L^1_3]Cl_4$	20 ± 3	6.5 ± 0.9	3.1
Δ - $[Fe_2L^{3a}]Cl_4$	13 ± 2	2.2 ± 0.2	5.7
cisPt	25 ± 4	2.6 ± 0.4	9.7

[a] The treatment was 72 h. The results are expressed as mean values ± SD (μ M) from three independent experiments ($p < 0.002$). [b] F: the factor is defined as IC_{50} (NER efficient, CHO-K1)/ IC_{50} (NER-deficient, MMC-2).

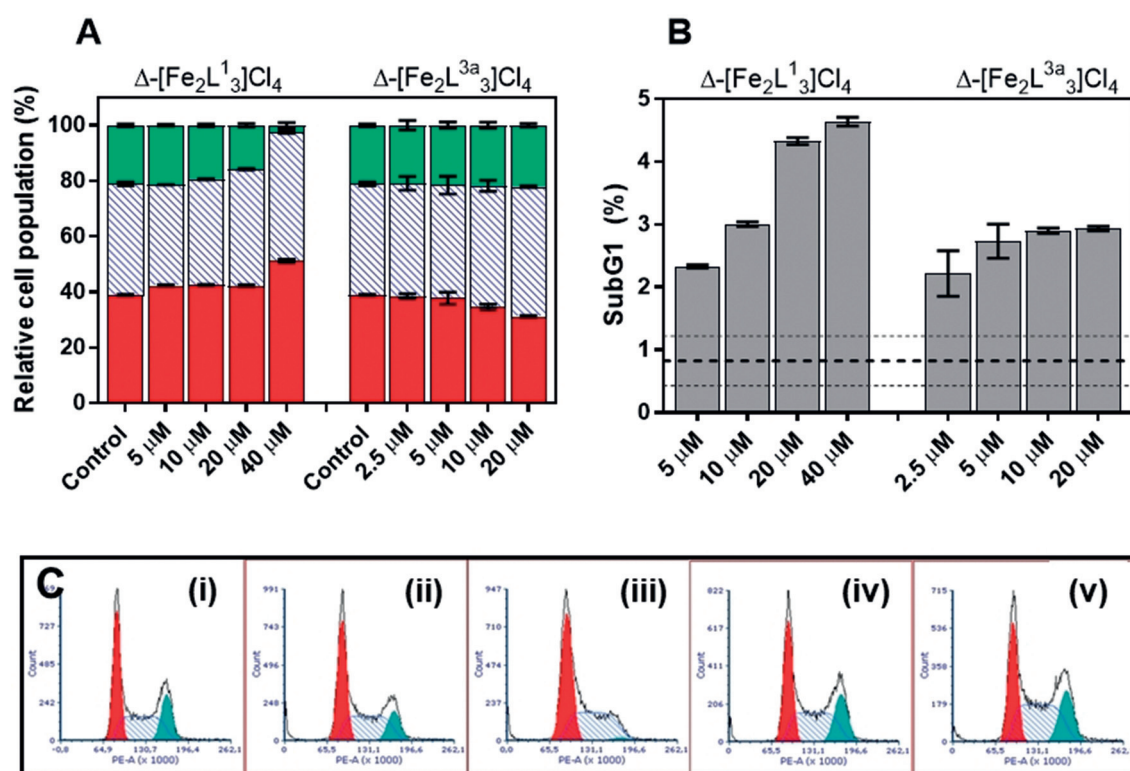


Figure 4. Cell cycle analysis in HCT116 p53^{+/+} cells. Effects of Δ -[Fe₂L¹₃]Cl₄ and Δ -[Fe₂L^{3a}₃]Cl₄ on cell-cycle profiles of HCT116 p53^{+/+} cells treated for 24 hours. A) Percentages of counts allocated to individual populations, G1 (red), S (blue dashed) and G2/M (green) of cells associated with sub-G1 phase. The dashed lines show the average value (with SD) of non-treated control. C) Cell cycle profiles. Effects of Δ -[Fe₂L¹₃]Cl₄ and Δ -[Fe₂L^{3a}₃]Cl₄ on cell-cycle profiles of HCT116 p53^{+/+} cells treated for 24 hours. (i) control, non-treated cells, (ii) 20 μ M Δ -[Fe₂L¹₃]Cl₄, (iii) 40 μ M Δ -[Fe₂L¹₃]Cl₄, (iv) 10 μ M Δ -[Fe₂L^{3a}₃]Cl₄ and (v) 20 μ M Δ -[Fe₂L^{3a}₃]Cl₄. The cells were stained with propidium iodide and assessed by FACS analysis. Red represents G1 phase, blue dashed S phase and green G2/M phase. Data were gained using FSC Express software.

Table 2: Antiproliferative activity data (IC₅₀) determined by MTT test for A2780 (wild-type), A2780cisR, HCT116 (wild-type, p53^{+/+}) and HCT116 p53^{-/-}.

Cell line	Δ -[Fe ₂ L ¹ ₃]Cl ₄	Δ -[Fe ₂ L ^{3a} ₃]Cl ₄	cisPt
A2780 ^[a]	15 ± 3	1.4 ± 0.3	3.3 ± 0.2
A2780cisR ^[a]	13 ± 3	1.2 ± 0.1	20 ± 3
HCT116 p53 ^{+/+} ^[b]	21 ± 1 ^[c]	7 ± 1	3.3 ± 0.4 ^[c]
HCT 116 p53 ^{-/-} ^[b]	8 ± 4 ^[c]	11 ± 2	7.5 ± 0.2 ^[c]

[a] The drug exposure time was 72 h. [b] The drug exposure time was 96 h. [c] Data previously published in reference [1d]. The results are expressed as IC₅₀ mean values ± SD (μ M) from three independent experiments.

effects on the cells via a different mechanism to cisplatin, whilst indicating a non-destructive interaction with DNA, more so for Δ -[Fe₂L^{3a}₃]Cl₄.

Biophysical studies in vitro

Given the above observations, we investigated the in vitro DNA-binding of Δ -[Fe₂L¹₃]Cl₄ and Δ -[Fe₂L^{3a}₃]Cl₄ via a fluorescence competition assay.^[33] The behavior was very similar for both compounds (Figure S19) with log K_{app} = 6.3 ± 0.1 and 6.1 ± 0.1 for Δ -[Fe₂L¹₃]Cl₄ and Δ -[Fe₂L^{3a}₃]Cl₄ respectively.

Thus DNA-binding affinity is not responsible for the higher accumulation of Δ -[Fe₂L^{3a}₃]Cl₄ in the nucleus.

Further, linear dichroism (LD) studies indicate that the complexes bind to naked calf thymus DNA in a specific orientation, probably the major groove.^[1a] These results, alongside the negative comet assays suggest that the DNA interactions are non-covalent, and probably reversible, akin to those of peptide α -helices and zinc fingers.^[34,35]

In vivo studies

Based on their potency and selectivity, Δ -[Fe₂L¹₃]Cl₄ and Δ -[Fe₂L^{3a}₃]Cl₄ were selected for initial in vivo evaluation. They were administered as a single intravenous (IV) injection in HCT116 p53^{-/-} bearing athymic nude mice. Prior to these studies, the maximum tolerated dose (MTD) was determined for both compounds; the glucose-appended metallohelix Δ -[Fe₂L^{3a}₃]Cl₄ (MTD = 1.75 mg kg⁻¹) was far better tolerated than Δ -[Fe₂L¹₃]Cl₄ (MTD = 0.3 mg kg⁻¹). Statistically significant tumour growth delays compared to the negative control group was seen for both compounds Δ -[Fe₂L¹₃]Cl₄ ($p < 0.05$), Δ -[Fe₂L^{3a}₃]Cl₄ ($p < 0.01$). A single injection of the parent triplex system Δ -[Fe₂L¹₃]Cl₄ inhibited the tumour growth by 2.6 d, whereas the glycosylated metallohelix Δ -[Fe₂L^{3a}₃]Cl₄ led to a growth delay of 4.3 d, that is, very similar to the

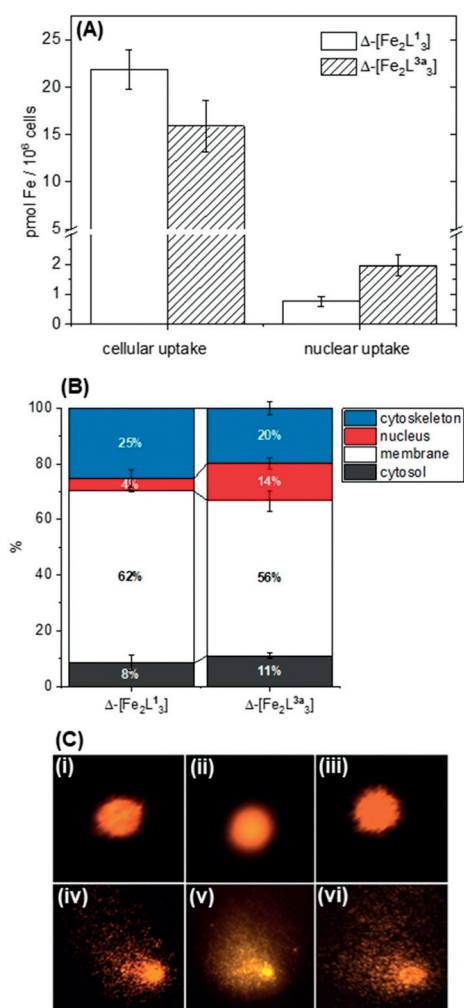


Figure 5. Cellular uptake, distribution and single-cell gel electrophoresis. A) Cellular and nuclear uptake of Δ -[Fe₂L¹]₃Cl₄ and Δ -[Fe₂L^{3a}]₃Cl₄ in HCT116 p53^{+/+} cells treated for 16 h at 5 μ M concentrations. Fe content was measured by ICP-MS, and Fe content measured in untreated control cells was subtracted from each measurement. Nuclear were isolated using a Nuclei EZ prep kit. B) Cellular distribution of Fe in HCT116 p53^{+/+} cells treated under the same conditions and processed into sub-cellular components using a FractionPREP cell fractionation kit. C) Single-cell gel electrophoresis (Comet assay) analysis. Top panels: analysis of DNA strand break induction in HCT116 p53^{+/+} cells untreated (i) or exposed to 20 μ M Δ -[Fe₂L¹]₃Cl₄ (ii) and 10 μ M Δ -[Fe₂L^{3a}]₃Cl₄ (iii) for 18 h. Bottom panels: analysis of DNA crosslink induction in untreated (iv) or cells treated with 20 μ M Δ -[Fe₂L¹]₃Cl₄ (v) and 10 μ M Δ -[Fe₂L^{3a}]₃Cl₄ (vi) for 18 h; after treatment the cells were exposed to hydrogen peroxide.

clinical drug agent cisplatin (Table 3, Figure 6). Importantly, no weight loss effects were observed following treatment with Δ -[Fe₂L¹]₃Cl₄ or of Δ -[Fe₂L^{3a}]₃Cl₄, whereas cisplatin induced a showed 6% loss of body weight in the first day following injection.

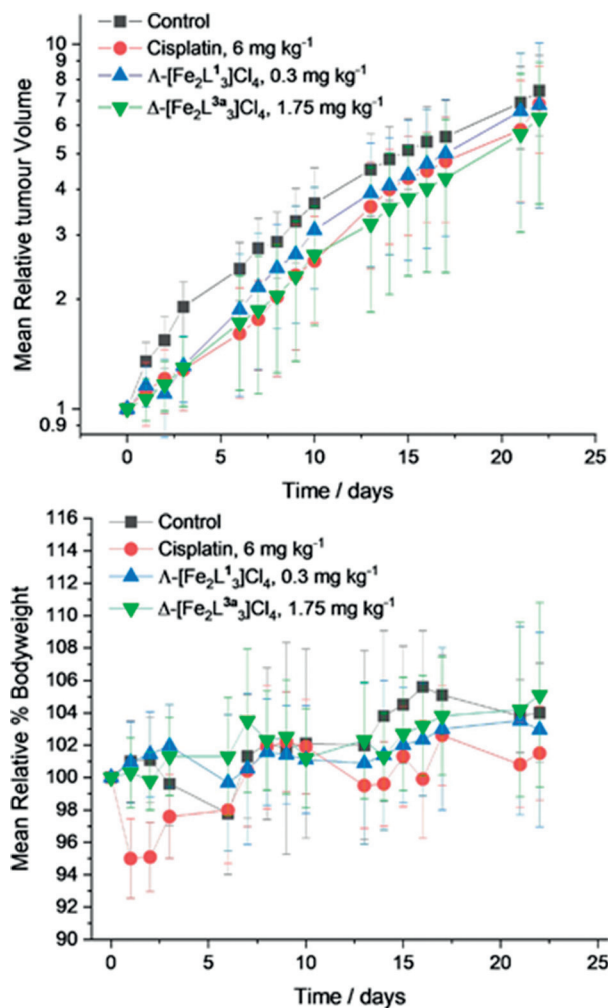


Figure 6. In vivo tumour studies. Tumour growth (top) and relative body weight (bottom) curves for [HCT116 p53^{-/-}]-tumour-bearing mice, administered with either nothing (control), 6 mg kg⁻¹ cisplatin (positive control), 0.3 mg kg⁻¹ Δ -[Fe₂L¹]₃Cl₄, or 1.75 mg kg⁻¹ Δ -[Fe₂L^{3a}]₃Cl₄. Mice were administrated with a single dose on day 0 by intravenous injection. Mean relative tumour volumes (A) and Mean relative body-weight (B) were measured at different time points, plotted, and expressed with \pm standard error; the significance *p* value < 0.01 was considered to be statistically significant (*n* = 8).

Conclusion

We have developed a very efficient method for the conjugation of triplex metallohelices with sugar units. The highly complex products have amphipathic structures, are optically pure, water-soluble, and extremely stable in water and biological media.

The addition of the carbohydrate units leads to substantial changes in the antiproliferative activity. Most strikingly, for the Δ -configured (right-handed helix) compounds, the apparent selectivity for cancer cells is greatly increased. In a mouse model, the drug tolerance and effect, as measured by MTD and tumour growth delay, are substantially improved versus the parent system. Encouragingly, no weight loss was recorded in the subjects following the dose.

Table 3: Efficacy study results.

Group	Relative tumour doubling time (days)	Growth delay (days)	Significance	Maximum % weight loss (day)
Δ -[Fe ₂ L ¹] ₃ Cl ₄ (0.3 mg kg ⁻¹)	6.8	2.6	$p < 0.05$	0
Δ -[Fe ₂ L ^{3a}] ₃ Cl ₄ (1.75 mg kg ⁻¹)	8.5	4.3	$p < 0.01$	0
Cisplatin (6 mg kg ⁻¹)	8.9	4.7	$p < 0.01$	6.0 (2)
Untreated controls	4.2	–	–	2.0 (6)

The triplex metallohelix system is also shown to be a rare example of a class of DNA-binding/aligning metallohelix. The parent and glycosylated compounds bind and align with DNA with very similar strength, thus validating our structural strategy of appending these polar units to the hydrophilic face of the helix, leaving the relatively hydrophobic ridge unperturbed.

In mechanistic terms, the addition of the glucose units leads to drug-like dose-dependent cell cycle effects, and the response observed in the cell cycle differs significantly between diastereoisomers of the metallohelices. Further, while the glucose derivative was found to be the most selective for the chosen cancer cell system, we conclude that this is not due to GLUT receptor targeting. Indeed, the cellular uptake is actually attenuated by addition of the sugars. Interestingly however, intranuclear transport is overall increased, perhaps by a sugar-mediated process.^[30c] Notably, the intranuclear transport, and the presumed DNA binding events in cellulose, do not lead to DNA damage.

Overall it would appear that the modification of triplex metallohelices in this way is worthy of investigation as a strategy for improvement of targeting and efficacy in this system, just as it is for the natural α -helical systems. Also, we can add this behaviour to a growing list of evidences that this class of molecule, with its many variants, share features with cationic antimicrobial and anticancer peptides.

In vivo evaluation was performed under contract at the Institute of Cancer Therapeutics UK under Home Office licence PPL 40/3670. Local ethical approval was obtained on 07 April 2016 by the Animal Welfare and Ethical Review Body (AWERB) of the University of Warwick (reference AWERB.26/15-16).

Acknowledgements

We thank the Warwick's Institute of Advanced Study for an Early Career Fellowship (HS). V.B., J.K., H.K., V.N. and J.P. acknowledge the support from the Czech Science Foundation, Grant 18-09502S. R.P. acknowledges University Research Funding from the University of Huddersfield to support multidisciplinary research.

Conflict of interest

The authors declare no conflict of interest.

Keywords: antitumor agents · glycoconjugates · metallohelices · nuclear delivery · self-assembly

- [1] a) S. E. Howson, A. Bolhuis, V. Brabec, G. J. Clarkson, J. Malina, A. Rodger, P. Scott, *Nat. Chem.* **2012**, *4*, 31–36; b) A. D. Faulkner, R. A. Kaner, Q. M. A. Abdallah, G. Clarkson, D. J. Fox, P. Gurnani, S. E. Howson, R. M. Phillips, D. I. Roper, D. H. Simpson, P. Scott, *Nat. Chem.* **2014**, *6*, 797–803; c) R. A. Kaner, S. J. Allison, A. D. Faulkner, R. M. Phillips, D. I. Roper, S. L. Shepherd, D. H. Simpson, N. R. Waterfield, P. Scott, *Chem. Sci.* **2016**, *7*, 951–958; d) H. Song, N. J. Rogers, S. J. Allison, V. Brabec, H. Bridgewater, H. Kostrhunova, L. Markova, R. M. Phillips, E. C. Pinder, S. L. Shepherd, L. S. Young, J. Zajac, P. Scott, *Chem. Sci.* **2019**, *10*, 8547–8557; e) D. H. Simpson, A. Hapeshi, N. J. Rogers, V. Brabec, G. J. Clarkson, D. J. Fox, O. Hrabina, G. L. Kay, A. K. King, J. Malina, A. D. Millard, J. Moat, D. I. Roper, H. Song, N. R. Waterfield, P. Scott, *Chem. Sci.* **2019**, *10*, 9708–9720; f) H. Song, N. J. Rogers, V. Brabec, G. J. Clarkson, J. P. C. Coverdale, H. Kostrhunova, R. M. Phillips, M. Postings, S. L. Shepherd, P. Scott, *Chem. Commun.* **2020**, <https://doi.org/10.1039/D0CC02429E>.
- [2] a) J.-M. Lehn, A. Rigault, J. Siegel, J. Harrowfield, B. Chevrier, D. Moras, *Proc. Natl. Acad. Sci. USA* **1987**, *84*, 2565–2569; b) A. C. Hotze, B. M. Kariuki, M. J. Hannon, *Angew. Chem. Int. Ed.* **2006**, *45*, 4839–4842; *Angew. Chem.* **2006**, *118*, 4957–4960; c) S. K. Vellas, J. E. Lewis, M. Shankar, A. Sagatova, J. D. Tyndall, B. C. Monk, C. M. Fitchett, L. R. Hanton, J. D. Crowley, *Molecules* **2013**, *18*, 6383–6407; d) C. R. Glasson, G. V. Meehan, C. A. Motti, J. K. Clegg, P. Turner, P. Jensen, L. F. Lindoy, *Dalton Trans.* **2011**, *40*, 10481–10490; e) I. Gamba, G. Rama, E. Ortega-Carrasco, J.-D. Maréchal, J. Martínez-Costas, M. Eugenio Vázquez, M. V. López, *Chem. Commun.* **2014**, *50*, 11097–11100.
- [3] S. E. Howson, L. E. Allan, N. P. Chmel, G. J. Clarkson, R. van Gorkum, P. Scott, *Chem. Commun.* **2009**, 1727–1729.
- [4] a) V. Brabec, S. E. Howson, R. A. Kaner, R. M. Lord, J. Malina, R. M. Phillips, Q. M. Abdallah, P. C. McGowan, A. Rodger, P. Scott, *Chem. Sci.* **2013**, *4*, 4407–4416; b) C. Zhao, H. Song, P. Scott, A. Zhao, H. Tateishi-Karimata, N. Sugimoto, J. Ren, X. Qu, *Angew. Chem. Int. Ed.* **2018**, *57*, 15723–15727; *Angew. Chem.* **2018**, *130*, 15949–15953; c) J. Malina, P. Scott, V. Brabec, *Nucleic Acids Res.* **2015**, *43*, 5297–5306.
- [5] D. E. Mitchell, G. Clarkson, D. J. Fox, R. A. Vipond, P. Scott, M. I. Gibson, *J. Am. Chem. Soc.* **2017**, *139*, 9835–9838.
- [6] Y. Guan, Z. Du, N. Gao, Y. Cao, X. Wang, P. Scott, H. Song, J. Ren, X. Qu, *Sci. Adv.* **2018**, *4*, 0.
- [7] D. Kalafatovic, E. Giralt, *Molecules* **2017**, *22*, 1929.
- [8] K. M. Stewart, K. L. Horton, S. O. Kelley, *Org. Biomol. Chem.* **2008**, *6*, 2242–2255.
- [9] a) N. Sakai, S. Matile, *J. Am. Chem. Soc.* **2003**, *125*, 14348–14356; b) T. Takeuchi, M. Kosuge, A. Tadokoro, Y. Sugiura, M. Nishi, M. Kawata, N. Sakai, S. Matile, S. Futaki, *ACS Chem. Biol.* **2006**, *1*, 299–303.
- [10] a) T. Utsugi, A. J. Schroit, J. Connor, C. D. Bucana, I. J. Fidler, *Cancer Res.* **1991**, *51*, 3062–3066; b) M. Dathé, M. Schümann, T. Wiprecht, A. Winkler, M. Beyermann, E. Krause, K. Matsuzawa

- ki, O. Murase, M. Bienert, *Biochemistry* **1996**, *35*, 12612–12622; c) S. Riedl, D. Zweytick, K. Lohner, *Chem. Phys. Lipids* **2011**, *164*, 766–781.
- [11] a) P. M. Fischer, *Med. Res. Rev.* **2007**, *27*, 755–795; b) G. Guidotti, L. Brambilla, D. Rossi, *Trends Pharmacol. Sci.* **2017**, *38*, 406–424; c) W. B. Kauffman, T. Fuselier, J. He, W. C. Wimley, *Trends Biochem. Sci.* **2015**, *40*, 749–764.
- [12] T. Johannssen, B. Lepenies, *Trends Biotechnol.* **2017**, *35*, 334–346.
- [13] a) E. Derivery, E. Bartolami, S. Matile, M. Gonzalez-Gaitan, *J. Am. Chem. Soc.* **2017**, *139*, 10172–10175; b) L. Kong, A. Almond, H. Bayley, B. G. Davis, *Nat. Chem.* **2016**, *8*, 461–469; c) L. Cai, Z. Gu, J. Zhong, D. Wen, G. Chen, L. He, J. Wu, Z. Gu, *Drug Discovery Today* **2018**, *23*, 1126–1138; d) A. Ardá, J. Jiménez-Barbero, *Chem. Commun.* **2018**, *54*, 4761–4769.
- [14] C. M. Taylor, *Tetrahedron* **1998**, *54*, 11317–11362.
- [15] a) M. R. Bond, J. A. Hanover, *J. Cell Biol.* **2015**, *208*, 869–880; b) X. Yang, K. Qian, *Nat. Rev. Mol. Cell Biol.* **2017**, *18*, 452–465.
- [16] P. M. Rudd, T. Elliott, P. Cresswell, I. A. Wilson, R. A. Dwek, *Science* **2001**, *291*, 2370–2376.
- [17] a) K. J. Doores, D. P. Gamblin, B. G. Davis, *Chem. Eur. J.* **2006**, *12*, 656–665; b) E. C. Calvaresi, P. J. Hergenrother, *Chem. Sci.* **2013**, *4*, 2319–2333.
- [18] a) E. Jones, R. Polt, *Front. Chem.* **2015**, *3*, 40; b) G. J. Mulder, *Trends Pharmacol. Sci.* **1992**, *13*, 302–304.
- [19] a) O. Warburg, *Science* **1956**, *123*, 309–314; b) O. Warburg, F. Wind, E. Negelein, *J. Gen. Physiol.* **1927**, *8*, 519.
- [20] a) M. Nomoto, K. Yamada, M. Haga, M. Hayashi, *J. Pharm. Sci.* **1998**, *87*, 326–332; b) J. F. Poduslo, G. L. Curran, *Mol. Brain Res.* **1994**, *23*, 157–162; c) D. Muthu, P. Robin, *Curr. Drug Delivery* **2005**, *2*, 59–73.
- [21] I. Gallego, A. Rioboo, J. J. Reina, B. Díaz, Á. Canales, F. J. Cañada, J. Guerra-Varela, L. Sánchez, J. Montenegro, *Chem-BioChem* **2019**, *20*, 1400–1409.
- [22] a) V. Percec, P. Leowanawat, H.-J. Sun, O. Kulikov, C. D. Nusbaum, T. M. Tran, A. Bertin, D. A. Wilson, M. Peterca, S. Zhang, *J. Am. Chem. Soc.* **2013**, *135*, 9055–9077; b) J. Tanaka, A. S. Gleinich, Q. Zhang, R. Whitfield, K. Kempe, D. M. Haddleton, T. P. Davis, S. Perrier, D. A. Mitchell, P. Wilson, *Biomacromolecules* **2017**, *18*, 1624–1633; c) O. G. Adesoye, I. N. Mills, D. P. Temelkoff, J. A. Jackson, P. Norris, *J. Chem. Educ.* **2012**, *89*, 943–945.
- [23] B. H. Lipshutz, B. R. Taft, *Angew. Chem. Int. Ed.* **2006**, *45*, 8235–8238; *Angew. Chem.* **2006**, *118*, 8415–8418.
- [24] J. C. Jewett, C. R. Bertozzi, *Chem. Soc. Rev.* **2010**, *39*, 1272–1279.
- [25] P. Liu, Y. Lu, X. Gao, R. Liu, D. Zhang-Negrerie, Y. Shi, Y. Wang, S. Wang, Q. Gao, *Chem. Commun.* **2013**, *49*, 2421–2423.
- [26] S. V. Moradi, W. M. Hussein, P. Varamini, P. Simerska, I. Toth, *Chem. Sci.* **2016**, *7*, 2492–2500.
- [27] R. Polt, M. Dhanasekaran, C. M. Keyari, *Med. Res. Rev.* **2005**, *25*, 557–585.
- [28] P. Varamini, F. M. Mansfeld, J. T. Blanchfield, B. D. Wyse, M. T. Smith, I. Toth, *J. Med. Chem.* **2012**, *55*, 5859–5867.
- [29] J.-P. Bapst, M. Calame, H. Tanner, A. N. Eberle, *Bioconjugate Chem.* **2009**, *20*, 984–993.
- [30] a) E. Duverger, V. Carpentier, A.-C. Roche, M. Monsigny, *Exp. Cell Res.* **1993**, *207*, 197–201; b) T. Lefebvre, S. Ferreira, L. Dupont-Wallois, T. Bussière, M.-J. Dupire, A. Delacourte, J.-C. Michalski, M.-L. Caillet-Boudin, *Biochim. Biophys. Acta Gen. Subj.* **2003**, *1619*, 167–176; c) M. Monsigny, C. Rondanino, E. Duverger, I. Fajac, A.-C. Roche, *Biochim. Biophys. Acta Gen. Subj.* **2004**, *1673*, 94–103.
- [31] E. R. Jamieson, S. J. Lippard, *Chem. Rev.* **1999**, *99*, 2467–2498.
- [32] H. Hall, J. Gurský, A. Nicodemou, I. Rybanská, E. Kimlíčková, M. Piršel, *Mutat. Res.* **2006**, *593*, 177–186.
- [33] J. Malina, M. J. Hannon, V. Brabec, *Nucleic Acids Res.* **2008**, *36*, 3630–3638.
- [34] S. A. Wolfe, L. Nekludova, C. O. Pabo, *Annu. Rev. Biophys. Biomol. Struct.* **2000**, *29*, 183–212.
- [35] N. P. Pavletich, C. O. Pabo, *Science* **1991**, *252*, 809–817.

Manuscript received: May 11, 2020

Accepted manuscript online: June 2, 2020

Version of record online: July 7, 2020